Electromagnetic Brain Mapping

Sylvain Baillet, John C. Mosher, and Richard M. Leahy

The past 15 years have seen tremendous advances in our ability to produce images of human brain function. Applications of functional brain imaging extend from improving our understanding of the basic mechanisms of cognitive processes to better characterization of pathologies that impair normal function. Magnetoencephalography (MEG) and electroencephalography (EEG) (MEG/EEG) localize neural electrical activity using noninvasive measurements of external electromagnetic signals. Among the available functional imaging techniques, MEG and EEG uniquely have temporal resolutions below 100 ms. This temporal precision allows us to explore the timing of basic neural processes at the level of cell assemblies. MEG/EEG source localization draws on a wide range of signal processing techniques including digital filtering, three-dimensional image analysis, array signal processing, image modeling and reconstruction, and, more recently, blind source separation and phase synchrony estimation. In this article we describe the underlying models currently used in MEG/EEG source estimation and describe the various signal processing steps required to compute these sources. In particular we describe methods for computing the forward fields for known source distributions and parametric and imaging-based approaches to the inverse problem.

Introduction

Functional brain imaging is a relatively new and multidisciplinary research field that encompasses techniques devoted to a better understanding of the human brain through noninvasive imaging of the electrophysiological, hemodynamic, metabolic, and neurochemical processes that underlie normal and pathological brain

1053-5888/01/$10.00©2001IEEE

function. These imaging techniques are powerful tools for studying neural processes in the normal working brain. Clinical applications include improved understanding and treatment of serious neurological and neuropsychological disorders such as intractable epilepsy, schizophrenia, depression, and Parkinson's and Alzheimer's diseases.

Brain metabolism and neurochemistry can be studied using radioactively labeled organic molecules, or probes, that are involved in processes of interest such as glucose metabolism or dopamine synthesis [1]. Images of dynamic changes in the spatial distribution of these probes, as they are transported and chemically modified within the brain, can be formed using positron emission tomography (PET). These images have spatial resolutions as high as 2 mm; however, temporal resolution is limited by the dynamics of the processes being studied, and by photon-counting noise, to several minutes. For more direct studies of neural activity, one can investigate local hemodynamic changes. As neurons become active, they induce very localized changes in blood flow and oxygenation levels that can be imaged as a correlate of neural activity. Hemodynamic changes can be detected using PET [1], functional magnetic resonance imaging (fMRI) [2], and transcranial optical imaging [3] methods. Of these, fMRI is currently the most widely used and can be readily performed using a standard 1.5T clinical MRI magnet, although an increasing fraction of studies are now performed on higher field (3-4.5T) machines for improved SNR and resolution. fMRI studies are capable of producing spatial resolutions as high as 1-3 mm; however, temporal resolution is limited by the relatively slow hemodynamic response, when compared to electrical neural activity, to approximately 1 s. In addition to limited temporal resolution, interpretation of fMRI data is hampered by the rather complex relationship between the blood oxygenation level dependent (BOLD) changes that are detected by fMRI and the underlying neural activity. Regions of BOLD changes in fMRI images do not necessarily correspond one-to-one with regions of electrical neural activity.

MEG and EEG are two complementary techniques that measure, respectively, the magnetic induction outside the head and the scalp electric potentials produced by electrical activity in neural cell assemblies. They directly measure electrical brain activity and offer the potential for superior temporal resolution when compared to PET or fMRI, allowing studies of the dynamics of neural networks or cell assemblies that occur at typical time scales on the order of tens of milliseconds [4]. Sampling of electromagnetic brain signals at millisecond intervals is readily achieved and is limited only by the multichannel analog-to-digital conversion rate of the measurements. Unfortunately, the spatial resolving power of MEG and EEG does not, in general, match that of PET and fMRI. Resolution is limited both by the relatively small number of spatial measurements—a few hundred in MEG or EEG versus tens of thousands or more in PET or fMRI—and the inherent ambiguity of the underlying static electromagnetic inverse problem. Only by placing restrictive models on the sources of MEG and EEG signals can we achieve resolutions similar to those of fMRI and PET.

Functional brain imaging is a multidisciplinary research field that encompasses techniques devoted to a better understanding of processes that underlie normal and pathological brain function.

Reviews of the application of MEG and EEG to neurology and neuropsychology can be found elsewhere [5]-[9]. We recommend [10] for a thorough review of MEG theory and instrumentation. This article provides a brief introduction to the topic with an overview of the associated inverse problem from a signal processing perspective. In the next two sections we describe the sources of MEG and EEG signals and how they are measured. Neural sources and head models are then described, followed by the various approaches to the inverse problem in which the properties of the neural current generators are estimated from the data. We conclude with a discussion of recent developments and our perspective on emerging signal processing issues for EEG and MEG data analysis.

Sources of EEG and MEG: Electrophysiological Basis

MEG and EEG are two techniques that exploit what Galvani, at the end of the 18th century, called "animal electricity," today better known as electrophysiology [11]. Despite the apparent simplicity in the structure of the neural cell, the biophysics of neural current flow relies on complex models of ionic current generation and conduction [12]. Roughly, when a neuron is excited by other—and possibly remotely located—neurons via an afferent volley of action potentials, excitatory postsynaptic potentials (EPSPs) are generated at its apical dendritic tree. The apical dendritic membrane becomes transiently depolarized and consequently extracellularly electronegative with respect to the cell soma and the basal dendrites. This potential difference causes a current to flow through the volume conductor from the nonexcited membrane of the soma and basal dendrites to the apical dendritic tree sustaining the EPSPs [13].

Some of the current takes the shortest route between the source and the sink by traveling within the dendritic trunk (see Fig. 1). Conservation of electric charges imposes that the current loop be closed with extracellular currents flowing even through the most distant part of the volume conductor. Intracellular currents are com-

monly called primary currents, while extracellular currents are known as secondary, return, or volume currents.

Both primary and secondary currents contribute to magnetic fields outside the head and to electric scalp potentials, but spatially structured arrangements of cells are of crucial importance to the superposition of neural currents such that they produce measurable fields. Macrocolumns of tens of thousands of synchronously activated large pyramidal cortical neurons are thus believed to be the main MEG and EEG generators because of the coherent distribution of their large dendritic trunks locally oriented in parallel, and pointing perpendicularly to the cortical surface [14]. The currents associated with the EPSPs generated among their dendrites are believed to be at the source of most of the signals detected in MEG and EEG because they typically last longer than the rapidly firing action potentials traveling along the axons of excited neurons [4]. Indeed, calculations such as those shown in [10] suggest each synapse along a dendrite may contribute as little as a 20 fA-m current source, probably too small to measure in MEG/EEG. Empirical observations instead suggest we are seeing sources on the order of 10 nA-m, and hence the cumulative summation of millions of synaptic junctions in a relatively small region. Nominal calculations of neuronal density and cortical thickness suggest that the cortex has a macrocellular current density on the order of 100 nA/mm^2 [10]. If we assume the cortex is about 4 mm thick, then a small patch 5 mm $\times$ 5 mm would yield a net current of 10 nA-m, consistent with empirical observations and invasive studies.

At a larger scale, distributed networks of collaborating and synchronously activated cortical areas are major contributors to MEG and EEG signals. These cortical areas are compatible with neuroscientific theories that model basic cognitive processes in terms of dynamically interacting cell assemblies [15]. Although cortical macrocolumns are assumed to be the main contributors to MEG and EEG signals [4], some authors have reported scalp recordings of deeper cortical structures including the hippocampus [16], cerebellum [17], and thalamus [18], [19].

Measuring EEG and MEG signals

Electroencephalography

EEG was born in 1924 when the German physician Hans Berger first measured traces of brain electrical activity in humans. Although today's electronics and software for EEG analysis benefit from the most recent technological developments, the basic principle remains unchanged from Berger's time. EEG consists of measurements of a set of electric potential differences between pairs of scalp electrodes. The sensors may be either directly glued to the skin (for prolonged clinical observation) at selected locations directly above cortical regions of interest or fitted in

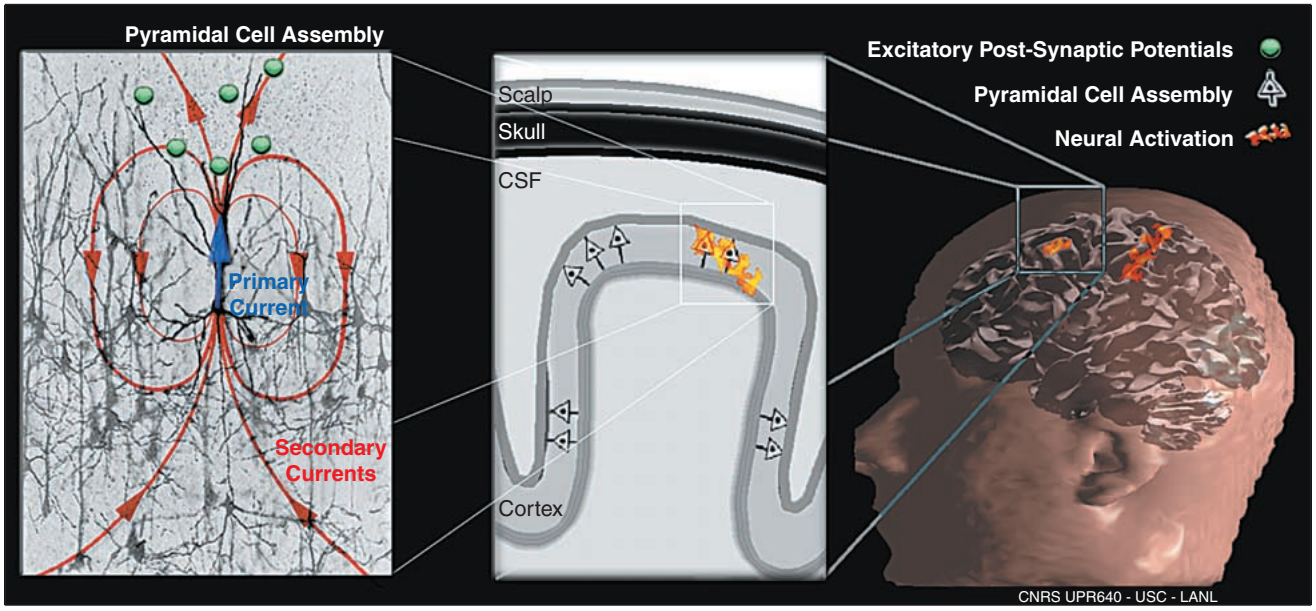

▲ *1. Networks of cortical neural cell assemblies are the main generators of MEG/EEG signals. Left: Excitatory postsynaptic potentials (EPSPs) are generated at the apical dendritic tree of a cortical pyramidal cell and trigger the generation of a current that flows through the volume conductor from the non-excited membrane of the soma and basal dendrites to the apical dendritic tree sustaining the EPSPs. Some of the current takes the shortest route between the source and the sink by travelling within the dendritic trunk (primary current in blue), while conservation of electric charges imposes that the current loop be closed with extracellular currents flowing even through the most distant part of the volume conductor (secondary currents in red). Center: Large cortical pyramidal nerve cells are organized in macro-assemblies with their dendrites normally oriented to the local cortical surface. This spatial arrangement and the simultaneous activation of a large population of these cells contribute to the spatio-temporal superposition of the elemental activity of every cell, resulting in a current flow that generates detectable EEG and MEG signals. Right: Functional networks made of these cortical cell assemblies and distributed at possibly mutliple brain locations are thus the putative main generators of MEG and EEG signals.*

an elastic cap for rapid attachment with near uniform coverage of the entire scalp. Research protocols can use up to 256 electrodes.

EEG has had tremendous success as a clinical tool, especially in studying epilepsy, where seizures are characterized by highly abnormal electrical behavior in neurons in epileptogenic regions. In many clinical and research applications, EEG data are analyzed using pattern analysis methods to associate characteristic differences in the data with differences in patient populations or experimental paradigm. The methods described here for estimating the location, extent and dynamic behavior of the actual current sources in the brain are currently less widely used in clinical EEG.

Though dramatic changes in the EEG, such as interictal spikes occurring between epileptic seizures, may be readily visible in raw measurements, event-related signals associated with, for example, presentation of a specific sensory stimulus or cognitive challenge, are often lost in background brain activity. Dawson demonstrated in 1937 that by adding stimulus-locked EEG traces recorded during several instances of the same stimulus, one could reveal spatio-temporal components of the EEG signal related with that stimulus, and background noise would be minimized. This method of "stimulus-locked" averaging of event-related EEG is now a standard technique for noise reduction in event-related studies.

Averaging, however, relies on the strong hypothesis that the brain is in a stationary state during the experiment with insignificant adaptation or habituation to experimental conditions during repeated exposure to a stimulus or task. In general, this stationarity does not hold true, especially as the number of trials increases, which has motivated new research approaches that study the inter-trial variations by greatly reducing the number of trials in each average, or by analyzing the raw unaveraged EEG data [20], [21].

Magnetoencephalography

Typical EEG scalp voltages are on the order of tens of microvolts and thus readily measured using relatively low-cost scalp electrodes and high-impedance high-gain amplifiers. In contrast, characteristic magnetic induction produced by neural currents is extraordinarily weak, on the order of several tens of femtoTeslas, thus necessitating sophisticated sensing technology. In contrast to EEG, MEG was developed in physics laboratories and especially in low-temperature and superconductivity research groups. In the late 1960s, J.E. Zimmerman co-invented the SQUID (Superconducting QUantum Interference Device)—a supremely sensitive amplifier that has since found applications ranging from airborne submarine sensing to the detection of gravitational waves—and conducted the first human magnetocardiogram experiment using a SQUID sensor at MIT. SQUIDs can be used to detect and quantify minute changes in the magnetic flux through magnetometer coils in a superconducting environment. D.S. Cohen, also at MIT, made the first MEG recording a few years later [22].

Recent developments include whole-head sensor arrays for the monitoring of brain magnetic fields at typically 100 to 300 locations. Noise is a major concern for MEG. Instrumental noise is minimized by the use of superconducting materials and immersing the sensing setup in a Dewar cooled with liquid helium. High-frequency perturbations such as radiofrequency waves are easily attenuated in shielded rooms made of successive layers of mu-metal, copper, and aluminum (Fig. 2). Low frequency artifacts created by cars, elevators, and other moving objects near the MEG system are attenuated by the use of gradiometers as sensing units. A gradiometer is the hardware combination of multiple magnetometers to physically mimic the computation of the spatial gradient of the magnetic induction in the vicinity of the head. Noise sources distant from the gradiometer produce magnetic fields with small spatial gradients and hence are effectively attenuated using this mechanism.

As with EEG, MEG has potentially important applications in clinical studies where disease or treatments affect spontaneous or event-related neural activity. Again, stimulus-locked averaging is usually required to reduce back-

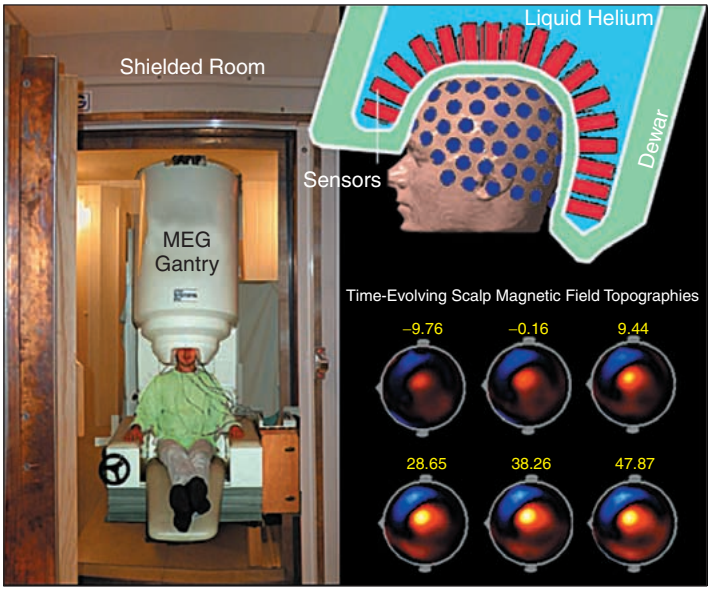

▲ *2. MEG instrumentation and typical signals. Typical scalp magnetic fields are on the order of a 10 billionth of the earth's magnetic field. MEG fields are measured inside a magnetically shielded room for protection against higher-frequency electromagnetic perturbations (left). MEG sensors use low-temperature electronics cooled by liquid helium (upper right) stored in a Dewar (left and upper right). Scalp magnetic fields are then recorded typically every millisecond. The resulting data can be visualized as time-evolving scalp magnetic field topographies (lower right). These plots display the time series of the recorded magnetic fields interpolated between sensor locations on the subject's scalp surface. This MEG recording was acquired as the subject moved his finger at time 0 (time relative to movement (t=0) is indicated in ms above every topography). Data indicate early motor preparation prior to the movement onset before peaking at about 20 ms after movement onset.*

The excellent time resolution of MEG and EEG gives us a unique window on the dynamics of human brain functions.

ground noise to a point where event-related signals can be seen in the data. The major attraction of MEG, as compared to EEG, is that while EEG is extremely sensitive to the effects of the secondary or volume currents, MEG is more sensitive to the primary current sources in which we are typically more interested—this will become clearer in our review of the forward model below. Contributors to the initial developments of MEG put great emphasis over the past two decades on the use of inverse methods to characterize the true sources of MEG signals within the brain. More recently, EEG and MEG have come to be viewed as complementary rather than competing modalities and most MEG facilities are equipped for simultaneous acquisition of both EEG and MEG data. As we shall see, inverse methods for the two are very closely related and can even be combined and optimized for joint source localization [23].

The Physics of MEG and EEG: Source and Head Models

Given a set of MEG or EEG signals from an array of external sensors, the inverse problem involves estimation of the properties of the current sources within the brain that produced these signals. Before we can make such an estimate, we must first understand and solve the forward problem, in which we compute the scalp potentials and external fields for a specific set of neural current sources.

Quasi-Static Approximation of Maxwell Equations

The useful frequency spectrum for electrophysiological signals in MEG and EEG is typically below 1 kHz, and most studies deal with frequencies between 0.1 and 100 Hz. Consequently, the physics of MEG and EEG can be described by the quasi-static approximation of Maxwell's equations. The quasi-static current flow $\boldsymbol{J}(\boldsymbol{r}')$ at location $\boldsymbol{r}'$ is therefore divergence free and can be related rather simply to the magnetic field $\boldsymbol{B}(\boldsymbol{r})$ at location $\boldsymbol{r}$ through the well-known Biot-Savart law

$$\boldsymbol{B}(\boldsymbol{r}) = \frac{\mu_0}{4\pi}\int \boldsymbol{J}(\boldsymbol{r}') \times \frac{\boldsymbol{r}-\boldsymbol{r}'}{\|\boldsymbol{r}-\boldsymbol{r}'\|^3} dv' \tag{1}$$

where μ_0 is the permitivity of free space. We can partition the total current density in the head volume into two current flows of distinct physiological significance: a primary (or driving) current flow $\boldsymbol{J}^P(\boldsymbol{r}')$ related to the original neural activity and a volume (or passive) current flow $\boldsymbol{J}^V(\boldsymbol{r}')$ that results from the effect of the electric field in the volume on extracellular charge carriers:

$$\begin{aligned}\boldsymbol{J}(\boldsymbol{r}') &= \boldsymbol{J}^p(\boldsymbol{r}') + \boldsymbol{J}^V(\boldsymbol{r}') = \boldsymbol{J}^p(\boldsymbol{r}') + \sigma(\boldsymbol{r}')\boldsymbol{E}(\boldsymbol{r}') \\ &= \boldsymbol{J}^p(\boldsymbol{r}') - \sigma(\boldsymbol{r}')\nabla V(\boldsymbol{r}')\end{aligned}$$

where $\sigma(\boldsymbol{r}')$ is the conductivity profile of the head tissues, which we will assume, for simplicity, to be isotropic, and, from the quasi-static assumption, the electric field $\boldsymbol{E}(\boldsymbol{r}')$ is the negative gradient of the electric potential, $V(\boldsymbol{r}')$.

If we assume that the head consists of a set of contiguous regions each of constant isotropic conductivity $\sigma_i, i = 1,\ldots,3$, representing the brain, skull and scalp for instance, we can rewrite the Biot-Savart law above as a sum of contributions from the primary and volume currents [10]:

$$\boldsymbol{B}(\boldsymbol{r}) = \boldsymbol{B}_0(\boldsymbol{r}) + \frac{\mu_0}{4\pi}\sum_{ij}(\sigma_i - \sigma_j)\int_{S_{ij}} V(\boldsymbol{r}')\frac{\boldsymbol{r}-\boldsymbol{r}'}{\|\boldsymbol{r}-\boldsymbol{r}'\|^3} \times d\boldsymbol{S}'_{ij}, \tag{2}$$

where $\boldsymbol{B}_0(\boldsymbol{r})$ is the magnetic field due to the primary current only. The second term is the volume current contribution to the magnetic field formed as a sum of surface integrals over the brain-skull, skull-scalp, and scalp-air boundaries.

This general equation states that the magnetic field can be calculated if we know the primary current distribution and the potential $V(\boldsymbol{r}')$ on all surfaces. We can create a similar equation for the potential itself, although the derivation is somewhat tedious [10], [24], yielding

$$\begin{aligned}(\sigma_i + \sigma_j)V(\boldsymbol{r}) &= 2\sigma_0 V_0(\boldsymbol{r}) \\ &\quad - \frac{1}{2\pi}\sum_{ij}(\sigma_i - \sigma_j)\int_{S_{ij}} V(\boldsymbol{r}')\frac{\boldsymbol{r}-\boldsymbol{r}'}{\|\boldsymbol{r}-\boldsymbol{r}'\|^3}\cdot d\boldsymbol{S}'_{ij}\end{aligned} \tag{3}$$

for the potential on surface $\boldsymbol{S}_{ij}$ where $V_0(\boldsymbol{r})$ is the potential at $\boldsymbol{r}$ due to the primary current distribution.

These two equations therefore represent the integral solutions to the forward problem. If we specify a primary current distribution $\boldsymbol{J}^P(\boldsymbol{r}')$, we can calculate a primary potential and a primary magnetic field,

$$\begin{aligned}V_0(\boldsymbol{r}) &= \frac{1}{4\pi\sigma_0}\int \boldsymbol{J}^P(\boldsymbol{r}')\cdot\frac{\boldsymbol{r}-\boldsymbol{r}'}{\|\boldsymbol{r}-\boldsymbol{r}'\|^3}d\boldsymbol{r}', \\ \boldsymbol{B}_0(\boldsymbol{r}) &= \frac{\mu_0}{4\pi}\int \boldsymbol{J}^P(\boldsymbol{r}')\times\frac{\boldsymbol{r}-\boldsymbol{r}'}{\|\boldsymbol{r}-\boldsymbol{r}'\|^3}d\boldsymbol{r}',\end{aligned} \tag{4}$$

the primary potential $V_0(\boldsymbol{r})$ is then used to solve (3) for the potentials on all surfaces, and therefore solves the forward problem for EEG. These surface potentials $V(\boldsymbol{r})$ and the primary magnetic field $\boldsymbol{B}_0(\boldsymbol{r})$ are then used to solve (2) for the external magnetic fields. Unfortunately, the solution of (3) has analytic solutions only for special shapes and must otherwise be solved numerically. We return to specific solutions of the forward problem below

but first we discuss the types of models used to describe the primary current distributions.

Source Models: Dipoles and Multipoles

Let us assume a small patch of activated cortex is centered at location $\boldsymbol{r}_q$ and that the observation point $\boldsymbol{r}$ is some distance away from this patch. The primary current distribution in this case can be well approximated by an equivalent current dipole represented as a point source $\boldsymbol{J}^P(\boldsymbol{r}') = \boldsymbol{q}\delta(\boldsymbol{r}'-\boldsymbol{r}_q)$, where $\delta(\mathbf{r})$ is the Dirac delta function, with moment $\boldsymbol{q} \equiv \int \boldsymbol{J}^P(\boldsymbol{r}')d\boldsymbol{r}'$. The current dipole is a straightforward extension of the better-known model of the paired-charges dipole in electrostatics. It is important to note that brain activity does not actually consist of discrete sets of physical current dipoles, but rather that the dipole is a convenient representation for coherent activation of a large number of pyramidal cells, possibly extending over a few square centimeters of gray matter.

The current dipole model is the workhorse of MEG/EEG processing since a primary current source of arbitrary extent can always be broken down into small regions, each region represented by an equivalent current dipole. This is the basis of the imaging methods described later on. However, an identifiability problem can arise when too many small regions and their dipoles are required to represent a single large region of coherent activation. These sources may be more simply represented by a multipolar model. The multipolar models can be generated by performing a Taylor series expansion of the Green's function $\boldsymbol{G}(\boldsymbol{r},\boldsymbol{r}') = \boldsymbol{r}-\boldsymbol{r}'/\|\boldsymbol{r}-\boldsymbol{r}'\|^3$ about the centroid of the source. Successive terms in the expansion give rise to the multipolar components: dipole, quadrupole, octupole, and so on. The first multipolar definitions for electrophysiological signals were established in magnetocardiography [25]. In MEG, the contributions to the magnetic field from octupolar and higher order terms drop off rapidly with distance, so that restricting sources to dipolar and quadrupolar fields is probably sufficient to represent most plausible cortical sources [26]. An alternative approach to multipolar models of brain sources can be found in [27].

Head Models

Spherical Head Models

Computation of the scalp potentials and induced magnetic fields requires solution of the forward equations (3) and (2), respectively, for a particular source model. When the surface integrals are computed over realistic head shapes, these equations must be solved numerically. Analytic solutions exist, however, for simplified geometries, such as when the head is assumed to consist of a set of nested concentric homogeneous spherical shells representing brain, skull, and scalp [28]-[30]. These models are routinely used in most clinical and research applications to MEG/EEG source localization.

Consider the special case of a current dipole of moment $\boldsymbol{q}$ located at $\boldsymbol{r}_q$ in a multishell spherical head, and an MEG system in which we measure only the radial component of the magnetic field, i.e., the coil surface of the magnetometer is oriented orthogonally to a radial line from the center of the sphere through the center of the coil. It is relatively straightforward to show that the contributions of the volume currents vanish in this case, and we are left with only the primary term $\boldsymbol{B}_0(\boldsymbol{r})$. Taking the radial component of this field for the current dipole reduces to the remarkably simple form:

$$B_r(\boldsymbol{r}) \equiv \frac{\boldsymbol{r}}{r}\cdot\boldsymbol{B}(\boldsymbol{r}) = \frac{\boldsymbol{r}}{r}\cdot\boldsymbol{B}_0(\boldsymbol{r}) = \frac{\mu_0}{4\pi}\frac{\boldsymbol{r}\times\boldsymbol{r}_q}{r\|\boldsymbol{r}-\boldsymbol{r}_q\|^3}\cdot\boldsymbol{q}. \tag{5}$$

Note that this magnetic field measurement is linear in the dipole moment $\boldsymbol{q}$ but highly nonlinear with respect to its location $\boldsymbol{r}_q$. Although we do not reproduce the results here, the magnetic fields for arbitrary sensor orientation and the scalp potentials for the spherical head models can both be written in a form similar to (5) as the inner product of a linear dipole moment with a term that is nonlinear in location [28]. While it may not be immediately obvious, this property also applies to numerical solution of (2) and (3), i.e., to arbitrary geometries of the volume conductor, and the measured fields remain linear in the dipole moment and nonlinear in the dipole location [10], [28].

From (5) we can also see that due to the triple scalar product, $B_r(\boldsymbol{r})$ is zero everywhere outside the head if $\boldsymbol{q}$ points towards the radial direction $\boldsymbol{r}_q$. A more general result is that radially oriented dipoles do not produce any external magnetic field outside a spherically symmetric volume conductor, regardless of the sensor orientation [31]. Importantly, this is not the case for EEG, which is sensitive to radial sources, constituting one of the major differences between MEG and EEG data.

Realistic Head Models

We have described how the forward models have closed-form solution for heads with conductivity profiles that can be modeled as a set of nested concentric homogeneous and isotropic spheres. In reality, of course, we do not have heads like this—our heads are anisotropic, inhomogeneous, and not spherical. Rather surprisingly, the spherical models work reasonably well, particularly for MEG measurements, which are less sensitive than EEG to the effects of volume currents, which, in turn, are affected more than primary currents by deviations from the idealized model [32].

More accurate solutions to the forward problem use anatomical information obtained from high-resolution volumetric brain images obtained with MR or X-ray computed tomography (CT) imaging. Since MR scans are now routinely performed as part of most MEG protocols, this data is readily available. To solve (2) and (3) we must extract surface boundaries for brain, skull, and scalp

One of the most exciting current challenges in functional brain mapping is the question of how to best integrate data from different modalities.

from these images. Many automated and semiautomated methods exist for surface extraction from MR images, e.g., [33], [34]. The surfaces can then be included in a boundary element method (BEM) calculation of the forward fields.

While this is an improvement on the spherical model, the BEM methods still assume homogeneity and isotropy within each region of the head. This ignores, for example, anisotropy in white matter tracts in the brain in which conduction is preferentially along the axonal fibers compared to the transverse direction. Similarly, the sinuses and diploic spaces in the skull make it very inhomogeneous, a factor that is typically ignored in BEM calculations. The finite element method (FEM) can deal with all of these factors and therefore represents a very powerful approach to solving the forward problem. Typically BEM and FEM calculations are very time consuming and use of these methods may appear impractical when incorporated as part of an iterative inverse solution. In fact, through use of fast numerical methods, precalculation, and look-up tables and interpolation of precalculated fields, both FEM and BEM can be made quite practical for applications in MEG and EEG [35].

One problem remains: these methods need to know the conductivity of the head. Most of the head models used in the bioelectromagnetism community consider typical values for the conductivity of the brain, skull, and skin. The skull is typically assumed to be 40 to 90 times more resistive than the brain and scalp, which are assumed to have similar conductive properties. These values are measured in vitro from postmortem tissue, where conductivity can be significantly altered compared to in vivo values [36]. Consequently, recent research efforts have focused on in vivo measures.

Electrical impedance tomography (EIT) proceeds by injecting a small current (1-10 microA) between pairs of EEG electrodes and measuring the resulting potentials at all electrodes. Given a model for the head geometry, EIT solves an inverse problem by minimizing the error between the measured potentials of the rest of the EEG leads and the model-based computed potentials, with respect to the parameters of the conductivity profile. Recent simulation results with three or four-shell spherical head models have demonstrated the feasibility of this approach though the associated inverse problem is also fundamentally ill-posed [37], [38]. These methods are readily extendible to realistic surface models as used in BEM calculations in which each region is assumed homogeneous, but it is unlikely that the EIT approach will be able to produce high-resolution images of spatially varying anisotropic conductivity.

A second approach to imaging conductivity is to use magnetic resonance. One technique uses the shielding effects of induced eddy currents on spin precession and could in principle help determine the conductivity profile at any frequency [39]. The second technique uses diffusion-tensor imaging with MRI (DT-MRI), which probes the microscopic diffusion properties of water molecules within the tissues of the brain [40]. The diffusion values can then be tentatively related to the conductivity of these tissues [41]. Both of these MR-based techniques are still under investigation, but given the poor signal-to-noise ratio (SNR) of the MR in bone regions, which is of critical importance for the forward EEG problem, the potential for fully three-dimensional impedance tomography with MR remains speculative.

Algebraic Formulation

With the introduction of the source and head models for solution of the forward problem, we can now provide a few key definitions and linear algebraic models that will clarify the different approaches taken in the inverse methods described in the next section. As we saw above, the magnetic field and scalp potential measurements are linear with respect to the dipole moment $\boldsymbol{q}$ and nonlinear with respect to the location r_q. For reasons of exposition it is convenient to separate the dipole magnitude $q \equiv \|\boldsymbol{q}\|$ from its orientation $\Theta = \boldsymbol{q} / \|\boldsymbol{q}\|$ which we represent in spherical coordinates by $\Theta = \{\theta, \varphi\}$. Let $m(\boldsymbol{r})$ denote either the scalp electric potential or magnetic field generated by a dipole:

$$m(\boldsymbol{r}) = a(\boldsymbol{r}, \boldsymbol{r}_q, \Theta) q, \tag{6}$$

where $a(\boldsymbol{r}, \boldsymbol{r}_q, \Theta)$ is formed as the solution to either the magnetic or electric forward problem for a dipole with unit amplitude and orientation Θ.

For the simultaneous activation of multiple dipoles located at $\boldsymbol{r}_{qi}$, and by linear superposition, we can simply sum the individual contributions to obtain $m(\boldsymbol{r}) = \sum_i a(\boldsymbol{r}, \boldsymbol{r}_{qi}, \Theta_i) q_i$. For the simultaneous EEG or MEG measurements made at N sensors we obtain

$$\boldsymbol{m} = \begin{bmatrix} m(\boldsymbol{r}_1) \\ \vdots \\ m(\boldsymbol{r}_N) \end{bmatrix} = \begin{bmatrix} a(\boldsymbol{r}_1, \boldsymbol{r}_{q1}, \Theta_1 & \cdots & a(\boldsymbol{r}_1, \boldsymbol{r}_{qp}, \Theta_p) \\ \vdots & \ddots & \vdots \\ a(\boldsymbol{r}_N, \boldsymbol{r}_{q1}, \Theta_1) & \cdots & a(\boldsymbol{r}_N, \boldsymbol{r}_{qp}, \Theta_p) \end{bmatrix} \begin{bmatrix} q_1 \\ \vdots \\ q_p \end{bmatrix}$$
$$= \boldsymbol{A}(\{\boldsymbol{r}_{qi}, \Theta_i\}) \boldsymbol{S}^T, \tag{7}$$

where $\boldsymbol{A}(\boldsymbol{r}_{\mathrm{qi}}, \Theta_i)$ is the gain matrix relating the set of p dipoles to the set of N discrete locations (now implicitly a function of the set of N sensor locations), m is a generic set of N MEG or EEG measurements, and the matrix $\boldsymbol{S}$ is a generalized matrix of source amplitudes, defined below. Each column of $\boldsymbol{A}$ relates a dipole to the array of sensor measurements and is called the forward field, gain vector,

or scalp topography, of the current dipole source sampled by the N discrete locations of the sensors. This model can be readily extended to include a time component t, when considering time evolving activities at every dipole location. For p sources and T discrete time samples, the spatio-temporal model can therefore be represented as

$$\boldsymbol{M} = \begin{bmatrix} m(\boldsymbol{r}_1,1) & \cdots & m(\boldsymbol{r}_1,T) \\ \vdots & \ddots & \vdots \\ m(\boldsymbol{r}_S,1) & \cdots & m(\boldsymbol{r}_S,T) \end{bmatrix} = \boldsymbol{A}\left(\{\boldsymbol{r}_i,\Theta_i\}\right) \begin{bmatrix} \boldsymbol{s}_1^T \\ \vdots \\ \boldsymbol{s}_p^T \end{bmatrix} = \boldsymbol{A}(\{\boldsymbol{r}_i,\Theta_i\})\boldsymbol{S}^T. \tag{8}$$

The corresponding time series for each dipole are the columns of the time series matrix S, where $\boldsymbol{S}^T$ indicates the matrix is transposed. Because the orientation of the dipole is not a function of time, this type of model is often referred to as a "fixed" dipole model. Alternative models that allow these dipoles to "rotate" as a function of time were introduced in [42] and are extensively reviewed in [43].

Imaging Electrical Activity in the Brain: The Inverse Problem

Parametric and imaging methods are the two general approaches to estimation of EEG and MEG sources. The parametric methods typically assume that the sources can be represented by a few equivalent current dipoles of unknown location and moment to be estimated with a nonlinear numerical method. The imaging methods are based on the assumption that primary sources are intracellular currents in the dendritic trunks of the cortical pyramidal neurons, which are aligned normally to the cortical surface. Thus a current dipole is assigned to each of many tens of thousands of tessellation elements on the cortical surface with the dipole orientation constrained to equal the local surface normal. The inverse problem in this case is linear, since the only unknowns are the amplitudes of the dipoles in each tessellation element. Given that the number of sensors is on the order of 100 and the number of unknowns is on the order of 10,000, the problem is severely underdetermined, and regularization methods are required to restrict the range of allowable solutions. In this section we will describe parametric and imaging approaches, contrasting the underlying assumptions and the limitations inherent in each.

Parametric Modeling

Least-Squares Source Estimation

In the presence of measurement errors, the forward model may be represented as $\boldsymbol{M} = \boldsymbol{A}(\{\boldsymbol{r}_{qi},\Theta_i\})\boldsymbol{S}^T + \varepsilon$, where ε is a spatio-temporal noise matrix. Our goal is to determine the set $\{\boldsymbol{r}_{qi},\Theta_i\}$ and the time series $\boldsymbol{S}$ that best describe our data. The earliest and most straightforward strategy is to fix the number of sources p and use a nonlinear estimation algorithm to minimize the squared error between the data and the fields computed from the estimated sources using a forward model. Each dipole represented in the matrix $\boldsymbol{A}(\{\boldsymbol{r}_{qi},\Theta_i\})$ comprises three nonlinear location parameters $\boldsymbol{r}_{qi}$, a set of two nonlinear orientation parameters $\Theta_i = (\theta_i, \phi_i)$, and the T linear dipole amplitude time series parameters in the vector $\boldsymbol{s}_i$.

For p dipoles, we define the measure of fit in the least-square (LS) sense as the square of the Frobenius norm

$$J_{LS}(\{\boldsymbol{r}_{qi},\Theta_i\},\boldsymbol{S}) = \left\|\boldsymbol{M} - \boldsymbol{A}(\{\boldsymbol{r}_{qi},\Theta_i\})\boldsymbol{S}^T\right\|_F^2. \tag{9}$$

A brute force approach is to use a nonlinear search program to minimize J_{LS} over all of parameters $(\{\boldsymbol{r}_{qi},\Theta_i\},\boldsymbol{S})$ simultaneously; however, the following simple optimal modification greatly reduces the computational burden. For any selection of $\{\boldsymbol{r}_{qi},\Theta_i\}$, the matrix $\boldsymbol{S}$ that will minimize J_{LS} is

$$\boldsymbol{S}^T = \boldsymbol{A}^+\boldsymbol{M}, \tag{10}$$

where $\boldsymbol{A}^+$ is the pseudoinverse of $\boldsymbol{A} = \boldsymbol{A}(\{\boldsymbol{r}_{qi},\Theta_i\})$. If $\boldsymbol{A}$ is of full column rank, then the pseudoinverse may be explicitly written as $\boldsymbol{A}^+ = (\boldsymbol{A}^T\boldsymbol{A})^{-1}\boldsymbol{A}^T$ [44], [45]. We can then solve (9) in $\{\boldsymbol{r}_{qi},\Theta_i\}$ by minimizing the adjusted cost function:

$$J_{LS}\left(\{\boldsymbol{r}_{qi},\Theta_i\}\right) = \left\|\boldsymbol{M} - \boldsymbol{A}(\boldsymbol{A}^+\boldsymbol{M})\right\|_F^2 = \left\|(\boldsymbol{I} - \boldsymbol{A}\boldsymbol{A}^+)\boldsymbol{M}\right\|_F^2 = \left\|\boldsymbol{P}_A^{\perp}\boldsymbol{M}\right\|_F^2, \tag{11}$$

where $\boldsymbol{P}_A^{\perp}$ is the orthogonal projection matrix onto the left null space of $\boldsymbol{A}$. Thus, the LS problem can be optimally solved in the limited set of nonlinear parameters $\{\boldsymbol{r}_{qi},\Theta_i\}$ with an iterative minimization procedure. The linear parameters in $\boldsymbol{S}$ are then optimally estimated from (10) [43], [45]. Minimization methods range from Levenberg-Marquardt and Nelder-Meade downhill simplex searches to global optimization schemes using multistart methods, genetic algorithms and simulated annealing [46].

This least-squares model can either be applied to a single snapshot or a block of time samples. When applied sequentially to a set of individual time slices, the result is called a "moving dipole" model, since the location is not constrained [47]. Alternatively, by using the entire block of data in the least-squares fit, the dipole locations can be fixed over the entire interval [42]. The fixed and moving dipole models have each proven useful in both EEG and MEG and remain the most widely used approach to processing experimental and clinical data.

A key problem with the LS method is that the number of sources to be used must be decided a priori. Estimates can be obtained by looking at the effective rank of the data using SVD or through information-theoretic criteria, but in practice expert data analysts often run several model orders and select results based on physiological plausibility. Caution is obviously required since a sufficiently large

number of sources can be made to fit any data set, regardless of its quality. Furthermore, as the number of sources increases, the nonconvexity of the cost function results in increased chances of trapping in undesirable local minima. This latter problem can be approached using stochastic or multistart search strategies [46], [48].

The alternatives described below avoid the nonconvexity issue by scanning a region of interest that can range from a single location to the whole brain volume for possible sources. An estimator of the contribution of each putative source location to the data can be derived either via spatial filtering techniques or signal classification indices. An attractive feature of these methods is that they do not require any prior estimate of the number of underlying sources.

Beamforming Approaches

A beamformer performs spatial filtering on data from a sensor array to discriminate between signals arriving from a location of interest and those originating elsewhere. Beamforming originated in radar and sonar signal processing but has since found applications in diverse fields ranging from astronomy to biomedical signal processing [49], [50].

Let us consider a beamformer that monitors signals from a dipole at location $\boldsymbol{r}_q$, while blocking contributions from all other brain locations. If we do not know the orientation of the dipole, we need a vector beamformer consisting of three spatial filters, one for each of the Cartesian axes, which we denote as the set $\{\Theta_1, \Theta_2, \Theta_3\}$. The output of the beamformer is computed as the three element vector $\boldsymbol{y}(t)$ formed as the product of a $3 \times N$ spatial filtering matrix $\boldsymbol{W}^T$ with $\boldsymbol{m}(t)$, the signal at the array at time t, i.e., $\boldsymbol{y}(t) = \boldsymbol{W}^T \boldsymbol{m}(t)$.

The spatial filter would ideally be defined to pass signals within a small distance δ of the location of interest $\boldsymbol{r}_q$ with a gain of unity while nulling signals from elsewhere [51]. Thus the spatial filter should obey the following constraints:

$$\boldsymbol{W}^T \boldsymbol{A}(\boldsymbol{r}) = \begin{cases} \boldsymbol{I} & \|\boldsymbol{r} - \boldsymbol{r}_q\| \le \delta: \text{ passband constraint} \\ \boldsymbol{0} & \|\boldsymbol{r} - \boldsymbol{r}_q\| > \delta: \text{ stopband constraint,} \end{cases} \tag{12}$$

where $\boldsymbol{A}(\boldsymbol{r}) = [\boldsymbol{a}(\boldsymbol{r}, \Theta_1), \boldsymbol{a}(\boldsymbol{r}, \Theta_2), \boldsymbol{a}(\boldsymbol{r}, \Theta_3)]$ is the $N \times 3$ forward matrix for three orthogonal dipoles at location r. There are insufficient degrees of freedom to enforce a strong stop-band constraint over the entire brain volume, so that a fixed spatial filter is impractical for this application.

Linearly constrained minimum variance (LCMV) beamforming provides an adaptive alternative in which the limited degrees of freedom are used to place nulls in the response at positions corresponding to interfering sources, i.e., neural sources at locations other than $\boldsymbol{r}_q$. This nulling is achieved by simply minimizing the output power of the beamformer subject to a unity gain constraint at the desired location $\boldsymbol{r}_q$. The LCMV problem can be written as

$$\min_{W^T} \operatorname{tr}\{C_y\} \text{ subject to } \boldsymbol{W}^T \boldsymbol{A}(\boldsymbol{r}_q) = \boldsymbol{I}, \tag{13}$$

where $\boldsymbol{C}_y = E[\boldsymbol{y}\boldsymbol{y}^T] = \boldsymbol{W}^T \boldsymbol{C}_m \boldsymbol{W}$ and $\boldsymbol{C}_m = E[\boldsymbol{m}\boldsymbol{m}^T]$. Solving (13) using the method of Lagrange multipliers yields the solution [49]:

$$\boldsymbol{W} = \left[\boldsymbol{A}(\boldsymbol{r}_q)^T \boldsymbol{C}_m^{-1} \boldsymbol{A}(\boldsymbol{r}_q)\right]^{-1} \boldsymbol{A}(\boldsymbol{r}_q)^T \boldsymbol{C}_m^{-1}. \tag{14}$$

Applying this filter to each of the snapshot vectors $\boldsymbol{m}(t), t = 1, \ldots, T$, in the data matrix $\boldsymbol{M}$ produces an estimate of the dipole moment of the source at $\boldsymbol{r}_q$ [51]-[53]. By simply changing the location $\boldsymbol{r}_q$ in (13), we can produce an estimate of the neural activity at any location.

Unfortunately, the transient and often correlated nature of neural activation in different parts of the brain will often limit performance of the LCMV as correlations between different sources will result in partial signal cancellation. However, simulation results [51], [54] and recent evaluations on real data [55] seem to indicate LCMV-based beamforming methods are robust to moderate levels of source/interference correlation. Similarly, modeling errors in the constraint matrix $\boldsymbol{A}(\boldsymbol{r}_q)$ or imprecise dipole locations can result in signal attenuation or even cancellation. More elaborate constraints may be designed by using eigenvectors that span a desired region to be either monitored (gain=1) or nulled (gain=0) [49], but as the number of constraints increases, the degrees of freedom are reduced and the beamformer becomes less adaptive to other unknown sources.

In the absence of signal, the LCMV beamformer will produce output simply due to noise. Because of the variable sensitivity of EEG and MEG as a function of source location, the noise gain of the filter will vary as a function of location $\boldsymbol{r}_q$ in the constraint $\boldsymbol{A}(\boldsymbol{r}_q)$. A strategy to account for this effect when using the LCMV beamformer in a scanning mode is to compute the ratio of the output variance of the beamformer to that which would have been obtained in the presence of noise only. It is straightforward to show that this ratio is given by

$$\operatorname{var}(\boldsymbol{r}_q) = \frac{\operatorname{tr}\left\{\left[\boldsymbol{A}(\boldsymbol{r}_q)^T \boldsymbol{C}_m^{-1} \boldsymbol{A}(\boldsymbol{r}_q)\right]^{-1}\right\}}{\operatorname{tr}\left\{\left[\boldsymbol{A}(\boldsymbol{r}_q)^T \boldsymbol{C}_\varepsilon^{-1} \boldsymbol{A}(\boldsymbol{r}_q)\right]^{-1}\right\}} \tag{15}$$

where $\boldsymbol{C}_\varepsilon$ is an estimate of the noise-only covariance [53]. This neural activity index can be extended to statistical parametric mapping (SPM) as in the synthetic aperture magnetometry (SAM) technique [53]; the recent parametric mapping method in [56] uses a similar idea to this, except that the linear operator applied to the data is a minimum-norm imaging, rather than spatial filtering, matrix. In low noise situations, the signal covariance can be ill-conditioned, and therefore the inverse may be regularized by replacing C_m^{-1} with $[\boldsymbol{C}_m + \lambda \boldsymbol{I}]^{-1}$ where λ is a small positive constant in (14) and (15) [53].

From Classical to RAP-MUSIC

The multiple signal classification approach (MUSIC) was developed in the array signal processing community [57] before being adapted to MEG/EEG source localization [43]. We will restrict our brief description of the MUSIC approach here to dipole sources with fixed orientation, although it can be extended to rotating dipoles and multipoles. As before, let $\boldsymbol{M} = \boldsymbol{A}(\{\boldsymbol{r}_{qi}, \Theta_i\})\boldsymbol{S}^T + \varepsilon$ be an $N \times T$ spatio-temporal matrix containing the data set under consideration for analysis, and let the data be a mixture of p sources. Let $\boldsymbol{M} = \boldsymbol{U}\Sigma\boldsymbol{V}^T$ be the singular value decomposition (SVD) of $\boldsymbol{M}$ [44]. In the absence of noise, the set of left singular vectors is an orthonormal basis for the subspace spanned by the data. Provided that $N > p$, the SNR is sufficiently large, and noise is i.i.d. at the sensors, one can define a basis for the signal and noise subspaces from the column vectors of $\boldsymbol{U}$. The signal subspace is spanned by the p first left singular vectors in $\boldsymbol{U}$, denoted $\boldsymbol{U}_S$, while the noise subspace is spanned by the remaining left singular vectors. The best rank p approximation of $\boldsymbol{M}$ is given by $\boldsymbol{M}_S = (\boldsymbol{U}_S \boldsymbol{U}_S^T)\boldsymbol{M}$ and $\boldsymbol{P}_S^{\perp} = \boldsymbol{I} - (\boldsymbol{U}_S \boldsymbol{U}_S^T)$ is the orthogonal projector onto the noise subspace.

We can define the MUSIC cost function as:

$$J(\boldsymbol{r}, \Theta) = \frac{\left\| \boldsymbol{P}_S^{\perp} \boldsymbol{a}(\boldsymbol{r}, \Theta) \right\|_2^2}{\left\| \boldsymbol{a}(\boldsymbol{r}, \Theta) \right\|_2^2}, \tag{16}$$

which is zero when $\boldsymbol{a}(\boldsymbol{r}, \Theta)$ corresponds to one of the true source locations and orientations, $\boldsymbol{r} = \boldsymbol{r}_{qi}$ and $\Theta = \Theta_i$, $i = 1, \ldots, p$ [43]. As in the beamforming approaches, an advantage over least-squares is that each source can be found by scanning through the possible set of locations and orientations, finding each source in turn, rather than searching simultaneously for all sources. By evaluating $\boldsymbol{J}(\boldsymbol{r}, \Theta)$ on a predefined set of grid points and then plotting its reciprocal, a "MUSIC" map is readily obtained with p peaks at or near the true locations of the p sources.

Although we do not show the details here, (16) can be modified to factor the dipole orientation out of the cost function. In this way, at each location we can test for the presence of a source without explicitly considering orientation. If a source is present, a simple generalized eigenanalysis of a 3×3 matrix is sufficient to compute the dipole orientation [43], [58]. Once all of the sources are found, their time series can be found, as in the least-squares approach, as $\boldsymbol{S}^T = \boldsymbol{A}^+ M$ where is the pseudoinverse of the gain matrix corresponding to the sources found in the MUSIC search.

Recursively applied and projected MUSIC (RAP-MUSIC) is a recent improvement to the original MUSIC scanning method, which refines the MUSIC cost function after each source is found by projecting the signal subspace away from the gain vectors $\boldsymbol{a}(\boldsymbol{r}_i, \Theta_i)$ corresponding to the sources already found [59]. Other extensions of MUSIC for MEG and EEG applications include the use of prewhitening to account for spatial correlations in background brain activity [60] and use of time-frequency methods to better select the signal subspace of interest [61].

One distinct advantage of MUSIC over LCMV methods is the relaxation of the requirement of orthogonality between distinct sources. MUSIC requires the weaker assumption that different sources have linearly independent time series. In noiseless data, partially correlated sources will still result in a cost function equal to zero at each true dipole location. In the presence of noise, MUSIC will fail when two sources are strongly or perfectly correlated. This problem can be corrected by adjusting the concept of single dipole models to specifically allow sets of synchronous sources [58].

Imaging Approaches

Cortically Distributed Source Models

Imaging approaches to the MEG/EEG inverse problem consist of methods for estimating the amplitudes of a dense set of dipoles distributed at fixed locations within the head volume. In this case, since the locations are fixed, only the linear parameters need to be estimated, and the inverse problem reduces to a linear one with strong similarities to those encountered in image restoration and reconstruction, i.e., the imaging problem involves solution of the linear system $\boldsymbol{M} = \boldsymbol{A}\boldsymbol{S}^T$ for the dipole amplitudes, $\boldsymbol{S}$.

The most basic approach consists of distributing dipoles over a predefined volumetric grid similar to the ones used in the scanning approaches. However, since primary sources are widely believed to be restricted to the cortex, the image can be plausibly constrained to sources lying on the cortical surface that has been extracted from an anatomical MR image of the subject [62]. Following segmentation of the MR volume, dipolar sources are placed at each node of a triangular tessellation of the surface of the cortical mantle. Since the apical dendrites that produce the measured fields are oriented normal to the surface, we can further constrain each of these elemental dipolar sources to be normal to the surface. The highly convoluted nature of the human cortex requires that a high-resolution representation contains on the order of ten to one hundred thousand dipole "pixels." The inverse problem is therefore hugely underdetermined and imaging requires the use of either explicit or implicit constraints on the allowed current source distributions. Typically, this has been accomplished through the use of regularization or Bayesian image estimation methods.

Bayesian Formulation of the Inverse Problem

For purposes of exposition, we will describe imaging methods from a Bayesian perspective. Consider the problem of estimating the matrix $\boldsymbol{S}$ of dipole amplitudes at each tessellation element from the spatio-temporal data matrix $\boldsymbol{M}$, which are related in the noiseless case by $\boldsymbol{M} = \boldsymbol{A}\boldsymbol{S}^T$. The ith row of $\boldsymbol{S}$ contains the amplitude image

across the cortex at time i. From Bayes theorem, the posterior probability for the amplitude matrix $\boldsymbol{S}$ conditioned on the data $\boldsymbol{M}$ is given by

$$p(\boldsymbol{S}/\boldsymbol{M}) = \frac{p(\boldsymbol{M}/\boldsymbol{S})\boldsymbol{p}(\boldsymbol{S})}{p(\boldsymbol{M})} \tag{17}$$

where $p(\boldsymbol{M}/\boldsymbol{S})$ is the conditional probability for the data given the image and $p(\boldsymbol{S})$ is a prior distribution reflecting our knowledge of the statistical properties of the unknown image. While Bayesian inference offers the potential for a full statistical characterization of the sources through the posterior probability [63], in practice images are typically estimated by maximization of the posterior or log-posterior probability:

$$\hat{\boldsymbol{S}} = \arg\max_{S} p(\boldsymbol{M}|\boldsymbol{S})\,p(\boldsymbol{S}) \equiv \arg\max_{S} \ln p(\boldsymbol{M}|\boldsymbol{S}) + \ln p(\boldsymbol{S}). \tag{18}$$

The term $p(\mathbf{M}/\mathbf{S})$ is the log likelihood for the data that depends on the forward model and the true source distribution. Typically, MEG and EEG data are assumed to be corrupted with additive Gaussian noise that we assume here is spatially and temporally white (generalizations for colored noise are straightforward). The log likelihood is then simply given by, within a constant,

$$\ln p(\boldsymbol{M}|\boldsymbol{S}) = \frac{1}{2\sigma^2}\left\|\boldsymbol{M} - \boldsymbol{A}\boldsymbol{S}^T\right\|_F^2. \tag{19}$$

The prior is a probabilistic model that describes our expectations concerning the statistical properties of the source for which we will assume an exponential density

$$p(\boldsymbol{S}) = \frac{1}{z}\exp\{-\beta f(\boldsymbol{S})\} \tag{20}$$

where β and z are scalar constants and $f(\boldsymbol{S})$ is a function of the image $\boldsymbol{S}$. This form encompasses both multivariate Gaussian models and the powerful class of Gibbs distributions or Markov random field models [64]. Combining the log likelihood and log prior gives the general form of the negative log posterior whose minimization yields the maximum a posteriori or MAP estimate:

$$U(\boldsymbol{S}) = \left\|\boldsymbol{M} - \boldsymbol{A}\boldsymbol{S}^T\right\|^2 + \lambda f(\boldsymbol{S}), \tag{21}$$

where $\lambda = 2\beta\sigma^2$. We can now give a brief overview of the imaging methods as special cases of minimization of the energy function in (21).

Linear Imaging Methods

In the case of a zero mean Gaussian image, the log prior has the form:

$$f(\boldsymbol{S}) = \mathrm{tr}\left\{\boldsymbol{S}\boldsymbol{C}_S^{-1}\boldsymbol{S}^T\right\}, \tag{22}$$

where $\boldsymbol{C}_S^{-1}$ is the inverse spatial covariance of the image; this model assumes that the image is independent from one time sample to the next. The corresponding energy function $U(\boldsymbol{S})$ is quadratic in $\boldsymbol{S}$ and the minimum is given by

$$\hat{\boldsymbol{S}}^T = \boldsymbol{W}\boldsymbol{W}^T\boldsymbol{A}^T\left(\boldsymbol{A}\boldsymbol{W}\boldsymbol{W}^T\boldsymbol{A}^T + \lambda\boldsymbol{I}\right)^{-1}\boldsymbol{M} = \boldsymbol{F}_\lambda\boldsymbol{M} \tag{23}$$

where we have factored $\boldsymbol{C}_S^{-1} = \boldsymbol{W}\boldsymbol{W}^T$. We note that for this case, the posterior is Gaussian and the MAP estimator is equivalent to the minimum mean squared error estimator or Wiener solution.

We can also interpret (21) as a Tikhonov regularized form of the inverse problem [65], [66], where the first term measures the fit to the data and the last is a regularizing function that measures smoothness of the image. The scalar λ is the regularization parameter that can be chosen using cross-validation methods or the L-curve. Within this regularized interpretation of (21), several forms of $\boldsymbol{W}$ have been proposed for MEG/EEG imaging applications:

- ▲ i) the identity matrix which produces a regularized minimum norm solution [67];
- ▲ ii) the column normalized minimum norm in which $\boldsymbol{W}$ is a diagonal matrix with elements equal to the norm of the corresponding column of $\boldsymbol{A}$ [68];
- ▲ iii) $\boldsymbol{W}$ computes a spatial derivative of the image of first order [69] or Laplacian form [70];
- ▲ iv) $\boldsymbol{W}$ is diagonal with elements equal to some estimate of the source power at that location, which may be computed from the output of a beamformer or MUSIC scan evaluated for each dipole pixel in turn [62], [71].

The underdetermined nature of the inverse problem in MEG/EEG is such that these linear methods produce very low-resolution solutions. Focal cortical sources tend to spread over multiple cortical sulci and gyri. In some applications, this may be sufficient to draw useful inferences from the resulting images. However, the images formed do not reflect the generally sparse focal nature of event-related cortical activation that is visualized using the other functional imaging modalities of PET and fMRI. In an attempt to produce more focal sources, the FOCUSS method [72] uses an iterative reweighting scheme in which the diagonal weight matrix $\boldsymbol{W}$ is updated at each iteration to equal the magnitude of the current image estimate. This approach does indeed produce sparse sources, but can be highly unstable with noisy data.

An interesting approach to the interpretation of minimum norm images formed using (23) was proposed by Dale et al. [56] in which an image of SNR is computed by normalizing each pixel value computed using (23) with an estimate of the noise sensitivity of that pixel, i.e., for the case of white Gaussian noise, each value in $\hat{\boldsymbol{S}}^T$ is normalized by the noise sensitivity given by the corresponding diagonal elements of $\boldsymbol{F}_\lambda\boldsymbol{F}_\lambda^T$. This has the interesting property of generally reducing the amount by which activity spreads across multiple sulci and gyri when compared to the standard minimum norm image; these images can also be used to make statistical inferences about the proba-

bility of a source being present at each location. This is an alternative to the statistical parametric mapping described in our discussion of beamforming methods.

Non-Gaussian Priors

In an attempt to produce more physiologically plausible images than can be obtained using linear methods, a large number of researchers have investigated alternative methods that can collectively be viewed as selecting alternative (nonquadratic) energy functions $f(\boldsymbol{S})$ in (21). From a regularization perspective, these have included entropy metrics and L_p norms with values of $p<2$, i.e., $f(\boldsymbol{S})=\|\boldsymbol{S}\|_p$ [73]. For the latter case, solutions will become increasingly sparse as p is reduced. For the special case of $p=1$, the problem can be modified slightly to be recast as a linear program. This is achieved by replacing the quadratic log-likelihood term with a set of underdetermined linear inequality constraints, where the inequalities reflect expected mismatches in the fit to the data due to noise. The L_1 cost can then be minimized over these constraints using a linear simplex algorithm. The attraction of this approach is that the properties of linear programming problems guarantee that there exists an optimal solution for which the number of nonzero pixels does not exceed the number of constraints, or equivalently the number of measurements. Since the number of pixels far outweighs the number of measurements, the solutions are therefore guaranteed to be sparse. This idea can be taken even further by using the L_p quasi-norm for values of $p<1$. In this case, it is possible to show that there exists a value $0<p<1$ for which the resulting solution is maximally sparse [68].

An alternative to the use of simple algebraic forms for the energy function $f(\boldsymbol{S})$ is to explicitly define a prior distribution that captures the desired statistical properties of the images. This can be done using the class of Markov random field (MRF) models [64], [74]. MRFs are a powerful framework, which have been extensively investigated in image restoration and reconstruction for statistical modeling of a range of image properties. A key property of MRFs is that their joint statistical distribution can be constructed from a set of potential functions defined on a local neighborhood system. Thus, the energy function $f(\boldsymbol{S})$ for the prior can be expressed as

$$f(\boldsymbol{S})=\sum_{j=1}^{J}\Phi_j(\boldsymbol{S}), \tag{24}$$

where $\Phi_j(\boldsymbol{S})$ is a function of a set of dipole pixel sites on the cortex that are all mutual neighbors. In this way, the MRF model can capture local interaction properties between image pixels and their neighbors. The total number, J, of these functions depends on the number of pixels and the number of different ways in which they are allowed to interact with their neighbors. Among the simplest MRF image models are those in which each of the potential functions involves a pair of neighboring pixel values. To model smoothness in images an appropriate choice of potential function might be the squared difference between these neighboring pixels.

In the case of MEG/EEG, the model should reflect the observation that cortical activation appears to exhibit a sparse focal structure, i.e., during an event related MEG/EEG study, most of the cortex is not involved in the response, and those areas correspond to focal regions of active cell assemblies. To capture these properties, a highly nonconvex potential function defined on the difference between each pair of neighboring pixel values was used in [75]. This prior has the effect of favoring the formation of small discrete regions of active cortex surrounded by regions of near-zero activity. An alternative model was proposed in [76] where a binary random field, x, was used to indicate whether each dipole pixel was either active ($x=1$) or inactive ($x=0$). A MRF was defined on this binary field to capture the two desired properties of sparseness and spatial clustering of active pixels; the parameters of this prior could then be adjusted to achieve differing degrees of sparseness and clustering [76]. Interactions between neighboring pixels can be described in both space and time. In [75] for instance, temporal smoothing is included in the prior in addition to the spatial sparseness term.

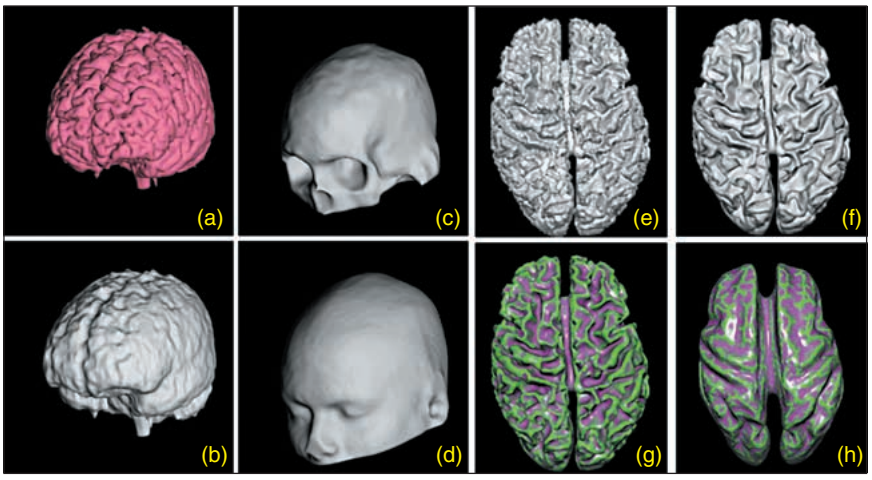

▲ *3. Examples of surfaces extracted from high-resolution MR images. The following surfaces were all extracted using an automated method described in [34]: (a) high-resolution brain surface, (b) smoothed brain surface, (c) skull surface, (d) scalp surface. The surfaces in (b), (c), and (d) are used as input to a boundary element code for computing forward MEG and EEG fields. The remaining figures are high-resolution cortical surfaces extracted from the same MR image and corrected to have the topology of a sphere. These can be used for cortically-constrained MEG or EEG imaging: (e) high resolution cortical surface, (f) smoothed representation obtained using relaxation methods similar to that described by [62] to allow improved visualization of deep sulcal features, (g) high resolution and (h) smoothed representations of the cortex with approximate measures of curvature overlaid. Figure courtesy of David W. Shattuck [90].*

The MRF-based image priors lead to nonconvex [75] and integer [76] programming problems in computing the MAP estimate. Computational costs can be very high for these methods since although the priors have computationally attractive neighborhood structures, the posteriors become fully coupled through the likelihood term. Furthermore, to deal with nonconvexity and integer programming issues some form of deterministic or stochastic annealing algorithms must be used [77].

Limitations of Imaging Approaches and Hybrid Alternatives

The imaging approaches are fundamentally limited by the huge imbalance between the numbers of spatial measurements and dipole-pixels. As we have seen, methods to overcome the resultant ambiguity range from minimum-norm based regularization to the use of physiologically based statistical priors. Nonetheless, we should emphasize that the class of images that provide reasonable fits to the data is very broad, and selection of the "best" image within the class is effectively done without regard

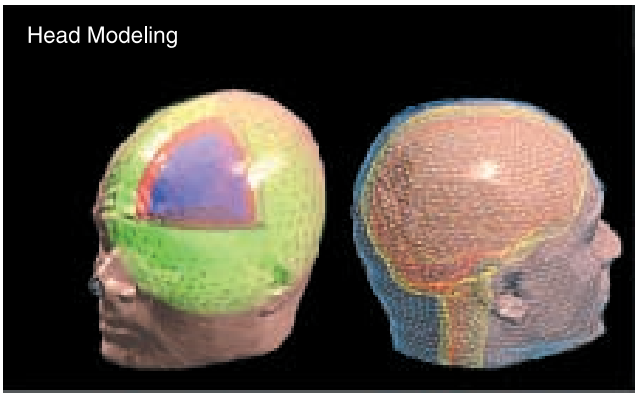

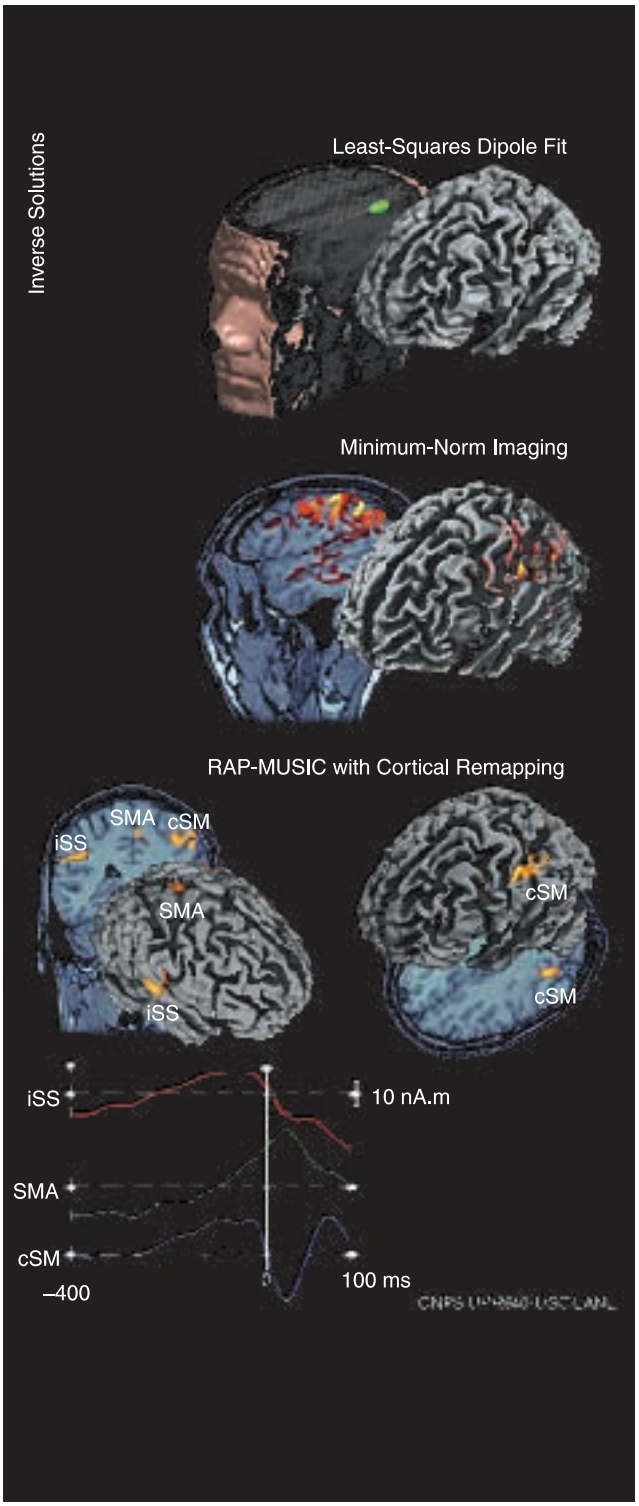

▲ *4. MEG, from modeling to imaging. Upper frame: The head modeling step consists in designing spherical (3-shell spherical volume conductor model; left) or realistic head models from the subject's anatomy using the individual MRI volume (piecewise homogenous BEM model, right). Right frame: Three representative imaging approaches were applied to identify the MEG generators associated to the right-finger movement data set introduced in Fig. 2. Top: The LS-fit approach produced a single-dipole model located inside the contralateral (left) central sulcus. Location is adequate but this model is too limited to make any assumption regarding the true spatial extension of the associated neural activation. The dipole time series (not shown here) indicated little premotor activation and much stronger somatosensory activity about 20 ms after the movement onset. Center: Minimum-Norm imaging of the cortical current density map has much lower spatial resolution. The estimated neural activation is spread all over the central sulcus region. Its extension to the more remote gyral crowns is certainly artifactual. The source time series in the central sulcus area (not shown here) revealed similar behavior as in the LS-fit case. Bottom: RAP-MUSIC modeling followed by cortical remapping: the RAP-MUSIC approach generated a 3-source model: one in the somatosensory regions of each hemispheres and one close to the post-supplementary motor area (SMA). Cortical remapping of the contralateral source revealed activation in the omega-shaped region of the primary sensory and motor hand areas (contralateral sensori-motor cortex, cSM). The cortical patch equivalent to the ipsilateral source was located in the ispsilateral somato-sensory region (iSS). Time series of the cortical activations were extracted in the [-400, 100] ms time window (bottom left). Sustained pre-motor activation occurred in all the above-mentioned areas; but only the SMA and cSM time series had clear peaks at about 20 ms following the movement onset, revealing motor activation of the contralateral finger and its associated somatosensory feedback. Premotor activation in the iSS could be related to active control of the immobility of the ipsilateral fingers.*

to the data. In contrast, the dipolar and multipolar methods control this ambiguity through a more explicit specification of the source model. This may lead to improved confidence in the estimated sources, but at the potential cost of missing sources that do not conform to the chosen model, and to the added complexity of interpreting the resulting solutions.

Recently we have been exploring the idea of remapping estimated dipolar and multipolar solutions onto cortex as a hybrid combination of the parametric and imaging approaches [78]. In this way, we can first rapidly find a solution to the inverse problem using, for example, the MUSIC scanning method. We then fit each source in turn to the cortex by solving a local imaging problem to compute an equivalent patch of activated cortex whose magnetic fields or scalp potentials match those of the estimated dipole or multipole (see Fig. 4 for an illustration on the data presented in Fig. 2).

A second hybrid approach to source estimation draws elements from the imaging and parametric approaches by specifying a prior distribution consisting of a set of activated cortical regions of unknown location, size and orientation. By constructing and sampling from a posterior distribution using Markov chain Monte Carlo methods, Schmidt et al. [79] are able to investigate the parameter space for this model and provide estimates, together with confidence values, of the true source distribution. As with the other physiologically based Bayesian models, this approach has high computational costs.

Emerging Signal Processing Issues

Combining fMRI and MEG/EEG

One of the most exciting current challenges in functional brain mapping is the question of how to best integrate data from different modalities. Since fMRI gives excellent spatial resolution with poor temporal resolution, while MEG/EEG gives excellent temporal resolution with poor spatial resolution, the data could be combined to provide insight that could not be achieved with either modality alone. One manner in which this has been done is to find regions of activation in fMRI images and use these to influence the formation of activated areas on the MEG/EEG images. This can be done by modifying the covariance matrix $\boldsymbol{C}_s^{-1}$ in (22) so that activated pixels in the fMRI images are more likely to be active in the MEG images [56]. This approach works exceedingly well when the areas of activation in the two studies actually correspond, but can lead to erroneous results if areas actively contributing to the MEG/EEG signal do not also produce activation in fMRI, or if hemodynamic response imaged with fMRI occurs at some distance from the electrical response measured with MEG/EEG [80]-[82]. The non-Gaussian Bayesian methods could be similarly modified to include fMRI information but would be subject to the same kind of errors. This issue remains an open research problem [83].

Signal Denoising and Blind Source Separation

An area of intense interest at the moment is the use of blind source separation and independent component analysis (ICA) methods for analysis of EEG and MEG data. Electrophysiological data is often corrupted by additive noise that includes background brain activity, electrical activity in the heart, eye-blink and other electrical muscle activity, and environmental noise. In general, these signals occur independently of either a stimulus, or the resultant event-related responses. Removal of these interfering signals is therefore an ideal candidate for ICA methods that are based on just such an independence assumption. Successful demonstrations of denoising have been published using mutual information [84], entropy [85], and fourth-order cumulant [86] based approaches. These methods perform best when applied to raw (unaveraged) data; one enticing aspect of this approach is that after noise removal, it may be possible to see event-related activity in the unaveraged denoised signals [87]. This is important since much of the information in MEG/EEG data, such as signals reflecting non time-locked synchronization between different cell assemblies [88] may be lost during the averaging process.

In addition to denoising, ICA has also been used to decompose MEG/EEG data into separate components, each representing physiologically distinct processes or sources. In principle, localization or imaging methods could then be applied to each of these components in turn. This decomposition is based on the underlying assumption of statistical independence between the activations of the different cell assemblies involved, which still remains to be validated experimentally. This approach could lead to interesting new ways of investigating data and developing new hypotheses for methods of neural communications. This is currently a very active and potentially fruitful research area.

Conclusion and Perspectives

As we have attempted to show, MEG/EEG source imaging encompasses a great variety of signal modeling and processing methods. We hope that this article serves as an introduction that will help to attract signal-processing researchers to explore this fascinating topic in more depth. We should emphasize that this article is not intended to be a comprehensive review, and for the purposes of providing a coherent introduction, we have chosen to present the field from the perspective of the work that we have done over the last several years.

The excellent time resolution of MEG/EEG gives us a unique window on the dynamics of human brain functions. Though spatial resolution is the Achilles' heel of this modality, future progress in modeling and applying modern signal processing methods may prove to make MEG/EEG a dependable functional imaging modality. Potential advances in forward modeling include better characterization of the skull, scalp and brain tissues from

MRI and in vivo estimation of the inhomogeneous and anisotropic conductivity of the head. Progress in inverse methods will include methods for combining MEG/EEG with other functional modalities and exploiting signal analysis methodologies to better localize and separate the various components of the brain's electrical responses. Of particular importance are methods for understanding the complex interactions between brain regions using single-trial signals to investigate transient phase synchronization between sensors [88] or directly within the MEG/EEG source map [89].

Acknowledgments

The authors are grateful to Marie Chupin and David W. Shattuck for their help in preparing the illustrations. This work was supported in part by the National Institute of Mental Health under Grant R01-MH53213, by the National Foundation for Functional Brain Imaging, Albuquerque, New Mexico, and by Los Alamos National Laboratory, operated by the University of California for the United States Department of Energy, under Contract W-7405-ENG-35.

Sylvain Baillet graduated in applied physics from the Ecole Normale Supérieure, Cachan and in signal processing from the University of Paris-Sud, in 1994. In 1998, he completed the Ph.D. program in electrical engineering from the University of Paris-Sud at the Institute of Optics, Orsay, and at the Cognitive Neuroscience and Brain Imaging Laboratory at La Salpêtrière Hospital, Paris. From 1998 to 2000 he was a Post-Doctoral Research Associate with the NeuroImaging group at the Signal and Image Processing Institute, University of Southern California, Los Angeles. He is now a Research Scientist with the National Center for Scientific Research (CNRS) and the Cognitive Neuroscience and Brain Imaging Laboratory, La Salpêtrière Hospital, Paris, France. His research interests involve methodological and modeling issues in brain functional imaging.

John C. Mosher received his bachelor's degree in electrical enginering with highest honors from the Georgia Institute of Technology in 1983. From 1979-1983 he was also a cooperative education student with Hughes Aircraft Company in Fullerton, CA. From 1983-1993, he worked at TRW in Los Angeles. While at TRW, he received his M.S. and Ph.D. degrees in electrical engineering from the Signal and Image Processing Institute of the University of Southern California. Upon graduation, he joined the Los Alamos National Laboratory, New Mexico, where he researches the forward and inverse modeling problems of electrophysiological recordings. His interests also include the general source localization and imaging problems, both in neuroscience work and in other novel applications of sensor technology.

Richard M. Leahy received the B.Sc. and Ph.D. degrees in electrical engineering from the University of Newcastle upon Tyne, U.K., in 1981 and 1985, respectively. In 1985 he joined the University of Southern California (USC), where he is currently a Professor in the Department of Electrical Engineering-Systems and Director of the Signal and Image Processing Institute. He holds joint appointments with the Departments of Radiology and Biomedical Engineering at USC and is an Associate Member of the Crump Institute for Molecular Imaging and the Laboratory for Neuro Imaging at UCLA. He is an Associate Editor of the *IEEE Transactions on Medical Imaging* and and was Co-Chair of the 2001 Conference on Information Processing in Medical Imaging. His research interests lie in the application of signal and image processing theory to biomedical inverse problems. His current research involves the development of methods for anatomical and functional imaging with applications in neuroimaging, oncology, and gene expression.

References

[1] S.R. Cherry and M.E. Phelps, "Imaging brain function with positron emission tomography," in *Brain Mapping: The Methods,* A.W. Toga and J.C. Mazziotta, Eds. New York: Academic, 1996.

[2] A. Villringer and B. Chance, "Noninvasive optical spectroscopy and imaging of human brain function," *Trends Neurosci.*, vol. 20, pp. 435-442, 1997.

[3] A.M. Howseman and R.W. Bowtell, "Functional magnetic resonance imaging: Imaging techniques and contrast mechanisms," *Philos. Trans. R. Soc. London B, Biol. Sci*., vol. 354, pp. 1179-1194, 1999.

[4] P.L. Nunez, *Electric Fields of the Brain*. New York: Oxford, 1981.

[5] C. Baumgartner, E. Pataraia, G. Lindinger, and L. Deecke, "Magnetoencephalography in focal epilepsy," *Epilepsia*, vol. 41, suppl. 3, pp. S39-47, 2000.

[6] C. Del Gratta, V. Pizzella, K. Torquati, and G.L. Romani, "New trends in magnetoencephalography," *Electroencephalogr. Clin. Neurophysiol. Suppl.*, vol. 50, pp. 59-73, 1999.

[7] R. Hari and N. Forss, "Magnetoencephalography in the study of human somatosensory cortical processing," *Philos. Trans. R. Soc. London B, Biol. Sci.*, vol. 354, pp. 1145-1154, 1999.

[8] V. Jousmaki, "Tracking functions of cortical networks on a millisecond timescale," *Neural Netw.*, vol. 13, pp. 883-889, 2000.

[9] M. Reite, P. Teale, and D.C. Rojas, "Magnetoencephalography: Applications in psychiatry," *Biol. Psychiatry*, vol. 45, pp. 1553-1563, 1999.

[10] M. Hämäläinen, R. Hari, R. Ilmoniemi, J. Knuutila, and O. Lounasmaa, "Magnetoencephalography. Theory, instrumentation and applications to the noninvasive study of human brain function," *Rev. Mod. Phys.*, vol. 65, pp. 413-497, 1993.

[11] M. Piccolino, "Luigi Galvani and animal electricity: Two centuries after the foundation of electrophysiology," *Trends Neurosci.,* vol. 20, pp. 443-448, 1997.

[12] A. Hodgkin, *The Conduction of the Nervous Impulse.* London, U.K.: Liverpool Univ. Press, 1964.

[13] P. Gloor, "Neuronal generators and the problem of localization in electroencephalography: Application of volume conductor theory to electroencephalography," *J. Clin. Neurophysiol.*, vol. 2, pp. 327-354, 1985.

[14] P.L. Nunez and R.B. Silberstein, "On the relationship of synaptic activity to macroscopic measurements: Does co-registration of EEG with fMRI make sense?," *Brain Topogr.*, vol. 13, pp. 79-96, 2000.

[15] F.J. Varela, "Resonant cell assemblies: A new approach to cognitive functions and neuronal synchrony," *Biol. Res.*, vol. 28, pp. 81-95, 1995.

[16] C.D. Tesche and J. Karhu, "THETA oscillations index human hippocampal activation during a working memory task," *Proc. Natl. Acad. Sci. USA*, vol. 97, pp. 919-924, 2000.

[17] C.D. Tesche and J. Karhu, "Somatosensory evoked magnetic fields arising from sources in the human cerebellum," *Brain Res.*, vol. 744, pp. 23-31, 1997.

[18] C.E. Tenke, C.E. Schroeder, J.C. Arezzo, and H.G. Vaughan, "Interpretation of high-resolution current source density profiles: A simulation of sublaminar contributions to the visual evoked potential," *Exp. Brain Res.*, vol. 94, pp. 183-192, 1993.

[19] R.R. Llinas, U. Ribary, D. Jeanmonod, E. Kronberg, and P.P. Mitra, "Thalamocortical dysrhythmia: A neurological and neuropsychiatric syndrome characterized by magnetoencephalography," *Proc. Natl. Acad. Sci. USA*, vol. 96, pp. 15222-15227, 1999.

[20] R. Vigario and E. Oja, "Independence: A new criterion for the analysis of the electromagnetic fields in the global brain?," *Neural Netw.*, vol. 13, pp. 891-907, 2000.

[21] P.A. Karjalainen, J.P. Kaipio, A. Koistinen, and M. Vauhkonen, "Subspace regularization method for the single trial analysis of evoked potentials," *IEEE Trans. Biomed. Eng.*, vol. 46, pp. 849-860, 1999.

[22] D. Cohen, "Magnetoencephalography: Evidence of magnetic fields produced by alpha rhythm currents," *Science*, vol. 161, pp. 664-666, 1972.

[23] S. Baillet, L. Garnero, G. Marin, and J.P. Hugonin, "Combined MEG and EEG source imaging by minimization of mutual information," *IEEE Trans. Biomed. Eng.*, vol. 46, pp. 522-534, 1999.

[24] D.B. Geselowitz, "On the magnetic field generated outside an inhomogeneous volume conductor by internal current sources," *IEEE Trans. Magn.*, pp. 346-347, 1970.

[25] T. Katila and P. Karp, "Magnetocardiography: Morphology and multipole presentations," *Biomagnetism, an Interdisciplinary Approach*, S.J. Williamson, G.L. Romani, L. Kaufman, and I. Modena, Eds. New York: Plenum, pp. 237-263, 1983.

[26] J.C. Mosher, R.M. Leahy, D.W. Shattuck, and S. Baillet, "MEG source imaging using multipolar expansions," in *Proc. 16th Conf. Information Processing in Medical Imaging,* IPMI'99, Visegrád, Hungary, June/July 1999 (*Lecture Notes in Computer Science*), A. Kuba, M. Sámal, and A. Todd-Pokropek, Eds. New York: Springer-Verlag, June/July 1999, pp. 15-28.

[27] G. Nolte and G. Curio, "Current multipole expansion to estimate lateral extent of neuronal activity: A theoretical analysis," *IEEE Trans. Biomed. Eng.*, vol. 47, pp. 1347-1355, 2000.

[28] J.C. Mosher, R.M. Leahy, and P.S. Lewis, "EEG and MEG: Forward solutions for inverse methods," *IEEE Trans. Biomed. Eng.*, vol. 46, pp. 245-259, 1999.

[29] J. de Munck, "The potential distribution in a layered spheroidal volume conductor," *J. Appl. Phys.*, vol. 64, pp. 464-470, 1988.

[30] Z. Zhang, "A fast method to compute surface potentials generated by dipoles within multilayer anisotropic spheres," *Phys. Med. Biol.*, vol. 40, pp. 335-349, 1995.

[31] J. Sarvas, "Basic mathematical and electromagnetic concepts of the biomagnetic inverse problem," *Phys. Med. Biol.*, vol. 32, pp. 11-22, 1987.

[32] R.M. Leahy, J.C. Mosher, M.E. Spencer, M.X. Huang, and J.D. Lewine, "A study of dipole localization accuracy for MEG and EEG using a human skull phantom," *Electroencephalogr. Clin. Neurophysiol.,* vol. 107, pp. 159-173, 1998.

[33] B. Fischl and A.M. Dale, "SURFER: A software package for cortical surface-based analysis and visualization," *NeuroImage*, vol. 9, no. 6, p. S243, 1999.

[34] D.W. Shattuck, S.R. Sandor-Leahy, K.A. Schaper, D.A. Rottenberg, and R.M. Leahy, "Magnetic resonance image tissue classification using a partial volume model," *NeuroImage*, vol. 13, no. 5, pp. 856-876, May 2001.

[35] J.J. Ermer, J.C. Mosher, S. Baillet, and R.M. Leahy, "Rapidly re-computable EEG forward models for realistic head shapes," *Phys. Med. Biol.*, vol. 46, no. 4, pp. 1265-1281, Apr. 2001.

[36] L. Geddes and L. Baker, "The specific resistance of biological materials—A compendium of data for the biomedical engineer and physiologist," *Med. Biol. Eng.*, vol. 5, pp. 271-293, 1967.

[37] T.C. Ferree, K.J. Eriksen, and D.M. Tucker, "Regional head tissue conductivity estimation for improved EEG analysis," *IEEE Trans. Biomed. Eng.*, vol. 47, pp. 1584-1592, 2000.

[38] S. Goncalves, J.C. de Munck, R.M. Heethaar, F.H. Lopes da Silva, and van B.W. Dijk, "The application of electrical impedance tomography to reduce systematic errors in the EEG inverse problem—A simulation study," *Physiol. Meas.*, vol. 21, pp. 379-393, 2000.

[39] Y. Yukawa, N. Iriguchi, and S. Ueno, "Impedance magnetic resonance imaging with external AC field added to main static field," *IEEE Trans. Magn.*, vol. 35, pp. 4121-4123, 1999.

[40] H.A. Rowley, P.E. Grant, and T.P. Roberts, "Diffusion MR imaging. Theory and applications," *Neuroimag. Clin. N. Am.*, vol. 9, pp. 343-361, 1999.

[41] D.S. Tuch, V.J. Wedeen, A.M. Dale, J.S. George, and J.W. Belliveau, "Conductivity mapping of biological tissue using diffusion MRI," *Ann. N. Y. Acad. Sci.*, vol. 888, pp. 314-316, 1999.

[42] M. Scherg and D. von Cramon, "Two bilateral sources of the late AEP as identified by a spatio-temporal dipole model," *Electroencephalogr. Clin. Neurophysiol.*, vol. 62, pp. 32-44, 1985.

[43] J. Mosher, P. Lewis, and R. Leahy, "Multiple dipole modeling and localization from spatio-temporal MEG data," *IEEE Trans. Biomed. Eng.*, vol. 39, pp. 541-557, 1992.

[44] G.H. Golub and C.F. Van Loan, *Matrix Computation*. Baltimore, MD: The John Hopkins Univ. Press, 1983.

[45] G.H. Golub and V. Pereyra, "The differentiation of pseudo-inverses and nonlinear least squares problems whose variables separate," *SIAM J. Numer. Anal.*, vol. 10, pp. 413-432, Apr. 1973.

[46] K. Uutela, M. Hamalainen, and R. Salmelin, "Global optimization in the localization of neuromagnetic sources," *IEEE Trans. Biomed. Eng.*, vol. 45, pp. 716-723, 1998.

[47] C.C. Wood, "Application of dipole localization methods to source identification in human evoked potentials," *Ann. N.Y. Acad. Sci.*, vol. 388, pp. 139-155, 1982.

[48] M. Huang, C. Aine, S. Supek, E. Best, D. Ranken, and E. Flynn, "Multi-start downhill simplex method for spatio-temporal source localization in magnetoencephalography," *Electroencephalogr. Clin. Neurophysiol.*, vol. 108, pp. 32-44, 1998.

[49] B.D. van Veen and K.M. Buckley, "Beamforming: A versatile approach to spatial filtering," *IEEE ASSP Mag.* (see also *IEEE Signal Processing Mag.*), vol. 5, pp. 4-23, Apr. 1988.

[50] H. Krim and M. Viberg, *IEEE Signal Processing Mag.*, vol. 13, pp. 67 -94, July 1996.

[51] B.D. van Veen, W. van Dronglen, M. Yuchtman, and A. Suzuki, "Localization of brain electrical activity via linearly constrained minimum variance spatial filtering," *IEEE Trans. Biomed. Eng.*, vol. 44, pp. 867-880, 1997.

[52] M. Spencer, R. Leahy, J. Mosher, and P. Lewis, "Adaptive filters for monitoring localized brain activity from surface potential time series," in *Conf. Rec. Twenty-Sixth Asilomar Conf. Signals, Systems and Computers*, vol. 1. Pacific Grove, CA: pp. 156-161, 1992.

[53] S.E. Robinson and J. Vrba, "Functional neuroimaging by Synthetic Aperture Magnetometry (SAM)," in *Recent Advances in Biomagnetism*, T. Yoshimoto, M. Kotani, S. Kuriki, H. Karibe, and N. Nakasato, Eds. Sendai, Japan: Tohoku Univ. Press, 1999, pp. 302-305.

[54] K.S. Sekihara, S.S. Nagarajan, D. Poeppel, and Y. Miyashita, "Spatio-temporal activities of neural sources from magnetoencephalographic data using

a vector beamformer," in *Proc. ICASSP-01*, Salt Lake City, UT, 2001., pp. 2021-2026.

[55] J. Gross, J. Kujala, M. Hamalainen, L. Timmermann, A. Schnitzler, and R. Salmelin, "Dynamic imaging of coherent sources: Studying neural interactions in the human brain," *Proc. Nat. Acad. Sci. USA*, vol. 98, pp. 694-699, 2001.

[56] A.M. Dale, A.K. Liu, B.R. Fischl, R.L. Buckner, J.W. Belliveau, J.D. Lewine, and E. Halgren, "Dynamic statistical parametric mapping: Combining fMRI and MEG for high-resolution imaging of cortical activity," *Neuron*, vol. 26, pp. 55-67, 2000.

[57] R.O. Schmidt, "Multiple emitter location and signal parameter estimation," *IEEE Trans. Antennas Propagat.*, vol. 34, pp. 276-280, 1986.

[58] J.C. Mosher and R.M. Leahy, "Recursive MUSIC: A framework for EEG and MEG source localization," *IEEE Trans. Biomed. Eng.*, vol. 45, pp. 1342-1354, 1998.

[59] J.C. Mosher and R.M. Leahy, "Source localization using recursively applied and projected (RAP) MUSIC," *IEEE Trans. Signal Processing*, vol. 47, pp. 332-340, 1999.

[60] K. Sekihara, S. Miyauchi, and H. Koizumu, "Covariance incorporated MEG-MUSIC algorithm and its application to detect SI and SII when large background brain activity exists," *NeuroImage*, vol. 3, no. 3, p. S92, 1996.

[61] K. Sekihara, S.S. Nagarajan, D. Poeppel, S. Miyauchi, N. Fujimaki, H. Koizumi, and Y. Miyashita, "Estimating neural sources from each time-frequency component of magnetoencephalographic data," *IEEE Trans. Biomed. Eng.*, vol. 47, pp. 642-653, 2000.

[62] A. Dale and M. Sereno, "Improved localization of cortical activity by combining EEG and MEG with MRI surface reconstruction: A linear approach," *J. Cogn. Neurosci.*, vol. 5, pp. 162-176, 1993.

[63] J.O. Berger, *Statistical Decision Theory and Bayesian Analysis*, 2nd ed. New York: Springer-Verlag, 1985.

[64] *Markov Random Fields: Theory and Applications,* R. Chellappa and A. Jain, Eds. San Diego, CA: Academic, 1991.

[65] G. Demoment, "Image reconstruction and restoration: Overview of common estimation structures and problems," *IEEE Trans. Acoust. Speech, Signal Processing*, vol. 37, pp. 2024-2036, 1989.

[66] A. Tikhonov and V. Arsenin, *Solutions to Ill-Posed Problems*. Washington D.C.: Winston, 1977.

[67] Y. Okada, "Discrimination of localized and distributed current dipole sources and localized single and multiple sources," *Biomagnetism, an Interdisciplinary Approach,* W. Weinberg, G. Stroink, and T. Katila, Eds. New York: Pergamon 1983, pp. 266-272.

[68] B. Jeffs, R. Leahy, and M. Singh, "An evaluation of methods for neuromagnetic image reconstruction," *IEEE Trans. Biomed. Eng.*, vol. 34, pp. 713-723, 1987.

[69] J.Z. Wang, S.J. Williamson, and L. Kaufman, "Magnetic source imaging based on the minimum-norm least-squares inverse," *Brain Topogr.*, vol. 5, 1993, pp. 365-371.

[70] R.M. Pascual-Marqui, C. Michel, and D. Lehman, "Low resolution electromagnetic tomography: A new method for localizing electrical activity in the brain," *Int. J. Psychophysiol.*, vol. 18, pp. 49-65, 1994.

[71] R. Greenblatt, "Probabilistic reconstruction of multiple sources in the bioelectromagnetic inverse problem," *Inverse Problems*, vol. 9, pp. 271-284, 1993.

[72] I.F. Gorodnitsky, J.S. Georg, and B.D. Rao, "Neuromagnetic source imaging with FOCUSS: A recursive weighted minimum norm algorithm," *Electroencephalogr. Clin. Neurophysiol.,* vol. 95, no. 4, pp. 231-251, Oct. 1995.

[73] K. Matsuura and Y. Okabe, "Selective minimum-norm solution of the biomagnetic inverse problem," *IEEE Trans. Biomed. Eng.*, vol. 8, pp. 608-615, 1995.

[74] S.Z. Li, *Markov Random Field Modeling in Computer Vision*. New York: Springer-Verlag, 1995.

[75] S. Baillet and L. Garnero, "A Bayesian approach to introducing anatomo-functional priors in the EEG /MEG inverse problem," *IEEE Trans. Biomed. Eng.*, vol. 44, pp. 374-385, 1997.

[76] J.W. Phillips, R.M. Leahy, and J.C. Mosher, "MEG-based imaging of focal neuronal current sources," *IEEE Trans. Med. Imag.*, vol. 16, pp. 338-348, 1997.

[77] S. Geman and D. Geman, "Stochastic relaxation, Gibbs distributions and the Bayesian restoration of images," *IEEE Trans. Pattern Anal. Machine Intell.*, PAMI-6, pp. 721-741, 1984.

[78] J.C. Mosher, S. Baillet, and R.M. Leahy, "EEG source localization and imaging using multiple signal classification approaches," *J. Clin. Neurophysiol.*, vol. 16, pp. 225-238, 1999.

[79] D. Schmidt, J. George, and C. Wood, "Bayesian inference applied to the electromagnetic inverse problem," *Hum. Brain Map.*, vol. 7, pp. 195-212, 1999.

[80] A. Puce, T. Allison, S.S. Spence, D.D. Spencer, and G. McCarthy, "Comparison of cortical activation evoked by face measured by intracranial field potentials and functional MRI: Two case studies," *Hum. Brain Map.*, vol. 5, pp. 298-305, 1997.

[81] A.J. Blood and A.W. Toga, "Optical intrinsic signal imaging responses are modulated in rodent somatosensory cortex during simultaneous whisker and forelimb stimulation," *J. Cereb. Blood Flow Metab.*, vol. 18, pp. 968-977, 1998.

[82] S.P. Ahlfors, G.V. Simpson, A.M. Dale, J.W. Belliveau, A.K. Liu, A. Korvenoja, J. Virtanen, M. Huotilainen, R.B. Tootell, H.J. Aronen, and R.J. Ilmoniemi , "Spatiotemporal activity of a cortical network for processing visual motion revealed by MEG and fMRI," *J. Neurophysiol.*, vol. 82, pp. 2545-2555, 1999.

[83] P.L. Nunez and R.B. Silberstein, "On the relationship of synaptic activity to macroscopic measurements: Does co-registration of EEG with fMRI make sense?," *Brain Topogr.*, vol. 13, pp. 79-96, 2000.

[84] T.W. Lee, M. Girolami, A.J. Bell, and T.J. Sejnowski, "A unifying information-theoretic framework for independent component analysis," *Comput. Math. Appl.*, vol. 39, pp. 1-21, 2000.

[85] A. Hyvarinen, "Fast ICA for noisy data using Gaussian moments," in *Proc. 1999 IEEE Int. Symp. Circuits and Systems VLSI*, vol. 5. Piscataway, NJ, 1999, pp. 57-61.

[86] J.F. Cardoso, "Blind signal separation: Statistical principles," *Proc. IEEE*, vol. 86, pp. 2009-2025, 1998.

[87] S. Makeig, M. Westerfield, T.P. Jung, J. Covington, J. Townsend, T.J. Sejnowski, and E. Courchesne, "Functionally independent components of the late positive event-related potential during visual spatial attention," *J. Neurosci*., vol. 19, pp. 2665-2680, 1999.

[88] E. Rodriguez, N. George, J.P. Lachaux, J. Martinerie, B. Renault, and F.J. Varela, "Perception's shadow: Long-distance synchronization of human brain activity," *Nature*, vol. 397, pp. 430-433, 1999.

[89] O. David, L. Garnero, and F.J. Varela, "A new approach to the MEG/EEG inverse problem for the recovery of cortical phase-synchrony," in *Proc. 17th Conf. Information Processing in Medical Imaging* (Lecture Notes in Computer Science, vol. LNCS2082), M. Insana and R Leahy, Eds. Springer, 2001, pp. 272-285.

[90] D.W. Shattuck, "Automated segmentation and analysis of human cerebral cortex imagery," Ph.D. dissertation, Univ. of Southern California, Aug. 2001.